Original Article

Institution of MECHANICAL ENGINEERS
Journal of AUTOMOBILE ENGINEERING

Proc IMechE Part D:
J Automobile Engineering
1–11

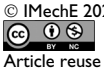

DOI: 10.1177/09544070251350178
journals.sagepub.com/home/pid
Sage

A fully active automotive suspension based on a rotary hydraulic valve

Pablo Tapia[1], Manfredi Tornabene[2,3], Giulia Moscone[2,3], Renato Galluzzi[1] and Nicola Amati[2,3]

Abstract

Active suspensions are commonly used in high-end vehicles to improve ride comfort and road holding. Commercial hydraulic active suspensions for cars typically employ directional solenoid valves to control hydraulic fluid flow, thereby modifying the dynamic behavior of output actuators. However, these valves require fast, accurate actuation, which is often hindered by their intrinsic nonlinear behavior. This research presents a fully active suspension based on the use of a novel rotary valve. The proposed design is compact and highly integrated with a permanent-magnet synchronous machine for precise position control. To test its validity, a prototype of the actuation system is simulated, built and tested. Experiments on the position control loop of the valve spool demonstrate that the proposed system is able to fulfill the necessary actuation bandwidth for an automotive suspension. Static and dynamic experiments on the actuator output validate the ability to yield forces in the four quadrants of the force-speed plane.

Keywords

Active suspension, chassis actuator, rotary valve, shock absorber, hydraulic actuator

Date received: 14 December 2024; accepted: 29 May 2025

Introduction

Vehicle suspension systems are fundamental to ensure both passenger comfort and vehicle stability, directly influencing the overall driving experience and safety. Most commercial light vehicles include passive hydraulic dampers with fixed characteristics that exhibit limited adaptability to a wide range of road conditions, maneuvering, or even user preferences. Furthermore, ride comfort and road holding are opposing objectives. This trade-off poses a significant design challenge, since enhancing ride comfort can lead to reduced stability and vice versa.[1]

To enhance adaptability to a wide range of travel conditions, active suspensions can be used. These actuators are capable of absorbing and exerting mechanical power on the suspension, thus attaining the desired comfort or road holding performances adapted to specific needs. The development of these systems has seen significant growth in the past two decades, emerging as a viable solution to the inherent limitations of traditional shock absorbers.[2–5]

Among active solutions, electromagnetic actuators stand out due to their operating principle. They typically feature an electric motor connected to each shock absorber through an ideally rigid transmission. Functional operation can be accomplished through linear motors in a direct-drive configuration[6–8] or through a suitable linear-to-rotary conversion mechanism.[9–11] Despite their favorable efficiency and actuation bandwidth, these devices are limited by the size of the electric motor, which usually constrains the force, and power capability of the device.

Alternatively, active suspensions based on hydraulic circuits can overcome the force and power limitations inherent in electromagnetic solutions. In these systems, a centralized pressure rail works together with directional valves that regulate the exerted or absorbed active force by channeling the power of the rail toward a linear hydraulic cylinder.[12,13] Hydraulic actuation solutions offer advantages in terms of modularity and

[1]School of Engineering and Sciences, Tecnologico de Monterrey, Mexico City, Mexico
[2]Department of Mechanical and Aerospace Engineering, Politecnico di Torino, Torino, Italy
[3]Center for Automotive Research and Sustainable Mobility (CARS), Politecnico di Torino, Torino, Italy

Corresponding author:
Renato Galluzzi, School of Engineering and Sciences, Tecnologico de Monterrey, Calle del Puente 222, Mexico City 14380, Mexico.
Email: renato.galluzzi@tec.mx

versatility because the pressure rail system can be installed in a suitable spot within the vehicle chassis. Corner actuation, on the other hand, is located on a very compact and lightweight valve able to regulate the amount of power delivered from the rail. Tier 1 manufacturer Tenneco has applied these solutions in their ACOCAR suspension system,[14] where a directional valve is integrated within the shock absorber. Babawuro et al. proposed a similar alternative through a four-way spool valve.[15]

Valves are typically a solenoid actuator capable of producing a linear displacement on a spool to vary the cross section for fluid passage.[16] The use of linear valves is common in oil-based and pneumatic active suspension systems.[17,18] Despite their popularity, these devices are highly nonlinear and hence, difficult to control and position accurately. To overcome these limitations, valves with rotary spools can be used, where accurate angular motion control is provided using conventional electric motors.[19] Fite et al.[20] implemented a four-way rotary valve with two inlet ports and two outflow ports for hot gas channeling. In semi-active suspension systems, the Dual Flow Valve[21] developed by Öhlins operates under a rotary actuation principle, establishing discrete, fixed apertures to impose a limited set of suspension damping behaviors.

Building on these advancements, this work proposes an active suspension system that takes advantage of inherent advantages of hydraulic technology. Corner actuation is performed using a novel valve concept with rotary spool, supplied by a two-rail pressure source. Then, the amount of force that the suspension exerts can be regulated by suitably controlling the angle of rotation.

To support this proposal, the sequel of this paper is organized as follows. First, the design of the rotary valve is outlined, including details about its working principle, hydraulics, actuation, assembly and control. Then, the simulation results demonstrate the functionality of the proposed actuator in a quarter-car vehicle model. Finally, experiments are performed on a prototype installed on dedicated testbeds in a laboratory setup.

Design

This work addresses the design of a new fully active suspension using a force actuator with a peak output force of 4 kN and maximum suspension speeds below 2 m/s. This design aims at an E-class luxury car. In the following, a design of the rotary valve for the suspension system is presented that can meet these requirements.

Working principle

The objective of this project is to develop a rotary spool active valve to establish a controllable pressure drop between fixed pressure rails and a hydraulic cylinder. This valve-equipped linear actuator replaces the passive damper on each corner of the vehicle. As such, the valve must be compact and highly integrated with the shock absorber.

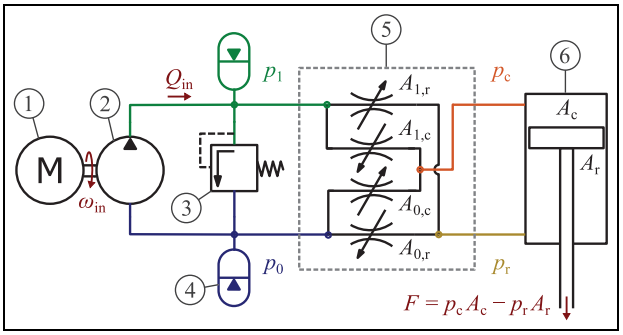

Figure 1. Proposed active suspension system: (1) electric motor, (2) hydraulic pump, (3) pressure-relief valve, (4) hydraulic accumulator (×2), (5) rotary valve, and (6) hydraulic cylinder.

A schematic view of the suspension actuation system is shown in Figure 1. The system comprises two fixed pressure ports (high pressure $p_1 = 45$ bar and low pressure $p_0 = 10$ bar) and two variable pressure ports connected to the damper compression chamber and the rebound chamber (labeled p_c and p_r, respectively). The pressure in inlet ports is established by a motor-pump unit and stabilized by means of two hydraulic accumulators. A pressure-relief valve is used to limit the pressure delta between p_1 and p_0. The hydraulic cylinder has a compression chamber cross section $A_c = 13\,\text{cm}^2$ and a rebound chamber cross section $A_r = 11\,\text{cm}^2$. All pressure ports are connected by means of variable orifices $A_{0,c}$ and $A_{1,c}$ for p_c, and $A_{0,r}$ and $A_{1,r}$ for p_r. Orifices exhibit reciprocal behavior with their respective pairs, as depicted by the sense of the arrows in Figure 1. For example, when the orifice $A_{1,r}$ is in the opening stage, its counterpart $A_{1,c}$ is closing simultaneously. Likewise, the pair made up of orifices $A_{0,c}$ and $A_{0,r}$ operates reciprocally. In practice, these four orifices are reproduced by a rotary spool and sleeve arrangement, as will be discussed later.

To better understand the described working principle of the valve, Figure 2 depicts two limit positions. An active extension force is achieved by fully opening the orifices $A_{1,c}$ and $A_{0,r}$, while their counterparts $A_{1,r}$ and $A_{0,c}$ remain closed. In the opposite valve condition ($A_{1,r}$ and $A_{0,c}$ open, $A_{1,c}$ and $A_{0,r}$ closed), a compression force is exerted.

Although Figure 2 illustrates limit conditions, it is intuitive to generalize the behavior toward a proportional law, where partial apertures may blend the rail pressures to attain specific forces in between maximum extension and compression values.

Hydraulic design

A rotary valve is designed to meet the actuation requirements described. The target orifice areas as a function of the angular position of the valve are plotted

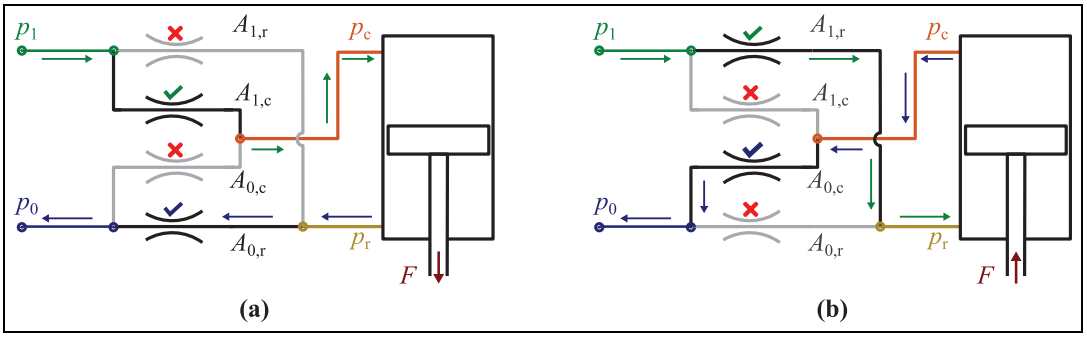

Figure 2. Extreme operating conditions of the valve to exert (a) an extension force, and (b) a compression force.

in Figure 3 for a total valve stroke of 30°. As previously stated, a complementary nature of the orifices connected to high-pressure ($A_{1,r}, A_{1,c}$) and low-pressure ($A_{0,r}, A_{0,c}$) rails is observed. In the center stroke, areas $A_{1,r}$ and $A_{1,c}$ have an overlap and an equal aperture at the null angular position. This configuration allows for the setting of equal pressure in the rebound and compression chambers of the hydraulic actuator, providing minimal active force on the vehicle suspension.

To facilitate the control task, the area transitions in Figure 3 are predominantly linear. In practice, the behavior of the described area is attained by means of the intersection between the slots machined in a cylindrical spool (rotating) and the holes prescribed on the surface of an annular sleeve (fixed). The latter element has the task of isolating the pressure chambers of the rail (p_1, p_0) and the actuator (p_r, p_c). In contrast, the spool acts as a connecting interface between the pressure chambers. The relative position between the spool and the sleeve defines the area of the four orifices as a function of the angular position of the spool, as seen in Figure 3. These multiple areas with significant size (up to 8 mm^2) are necessary to avoid an elevated pressure drop in the resulting orifices. In a preliminary analysis, geometries of linear and rotary valve layouts were studied to yield the shown target areas. This initial analysis revealed that, to attain the requested areas, the linear-displacement solution requires an axial length that is 150% larger than its rotary counterpart, with similar radial envelope. This limitation is due to the linear nature of solenoid actuation and the need to provide aperture through axial motion.

The spool and sleeve geometries of the final configuration of the rotary valve are illustrated in Figure 4. In addition to the interaction between the spool slots and the sleeve bores, a periodic pattern is exploited. This periodicity of order four is required to balance the radial forces of the fluid acting on the spool. Unbalanced effects increase the friction caused by the very tight radial clearance between the spool and the sleeve (10 μm).

As an example, Figure 4 also shows the results of the computational fluid dynamics (CFD) analysis of the rotary valve. For this task, the commercial software

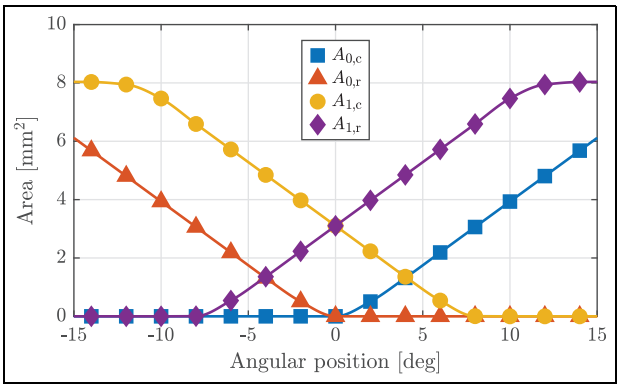

Figure 3. Target orifice areas as a function of the angular position of the valve.

Simerics Pumplinx was used. Valve operation is simulating by assigning rail boundary pressures ($p_0 = 10$ bar, $p_1 = 45$ bar) and proper boundary flow rates on the rebound and compression chambers of the actuator, respectively:

$$Q_r = A_r v \tag{1}$$

$$Q_c = A_c v \tag{2}$$

where v denotes the piston speed of the hydraulic cylinder. Actuator force is then calculated by measuring the pressure on the rebound and compression ports of the hydraulic cylinder:

$$F = p_c A_c - p_r A_r \tag{3}$$

The actuator performance is mainly characterized by the measurement of F at different spool angles and damper speed values. Other meaningful metrics include the radial forces produced on the spool surface and the torque due to the uneven pressure distribution along the spool. These quantities are related to the effort needed to rotate or fix the position of the spool.

For CFD simulations, the use of suspension mineral oil was assumed (mass density of 836 kg/m^3, dynamic viscosity of 9.7×10^{-3} Pas). The meshing of the fluid

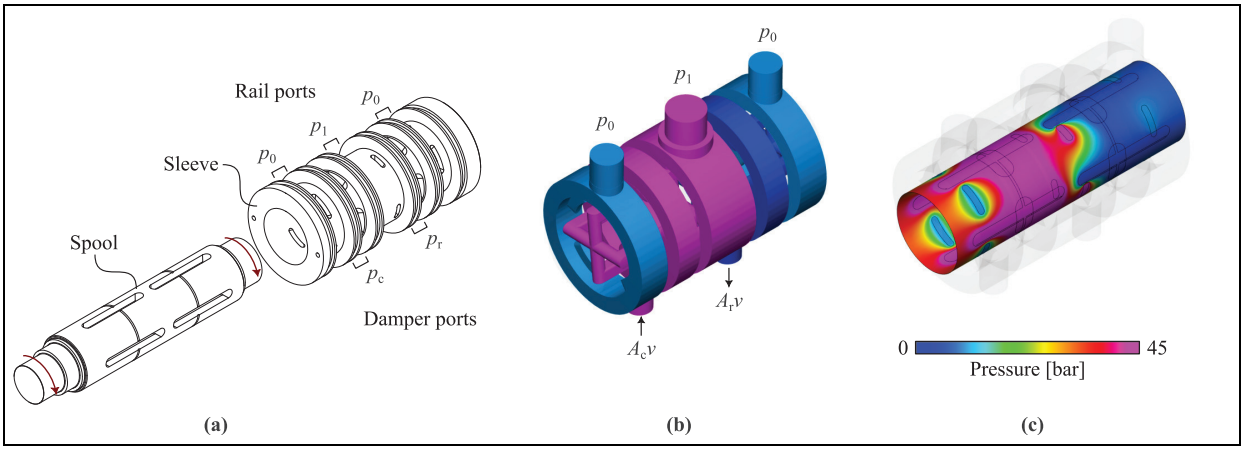

Figure 4. Rotary valve spool and sleeve: (a) geometry detail. CFD simulation example for a spool angle of −7° and actuator speed of 0.32 m/s to yield an active extension force: pressure distributions on (b) the spool and sleeve fluid domains, and (c) the radial gap between spool and sleeve.

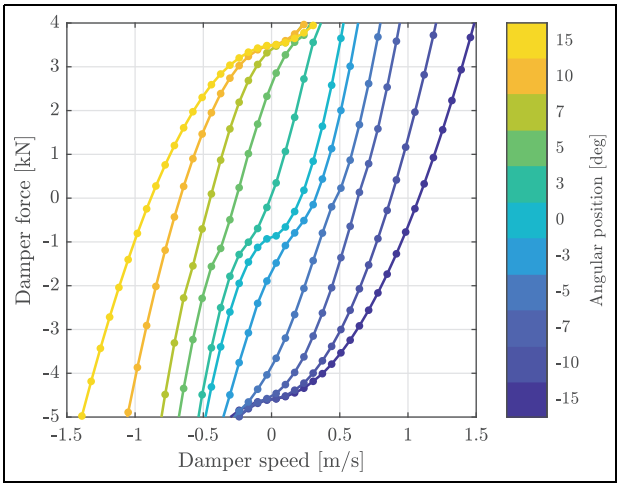

Figure 5. Actuator characteristic obtained from CFD simulations. The four-quadrant force-speed behavior of the actuator is determined for different angular positions of the valve spool. Quadrants ii and iv are active.

domains was established with prismatic cell elements with side lengths ranging from 0.2 to 5 mm, according to the refinement of the meshed geometries. In the case of the clearance region between the spool and the sleeve, four layers were stacked in the radial direction to accurately describe the leakage flow there.

This CFD simulation approach was applied to obtain the force-speed characteristic of the actuator in four quadrants, as observed in Figure 5.

Results show that, at null speed, the system can produce extension forces up to 4.75 kN and compression forces up to 3.65 kN. This force asymmetry is due to the difference in the cross sections of the pistons for the rebound and compression chambers. Thus, considering a force bias of 1.1 kN, the actuator is able to produce an active force of 4.2 kN in both directions. When the speed is increased, the active force decreases due to the presence of minor losses inside the hydraulic valve circuit. In contrast, the damping quadrants show increased forces as a result of the addition of these losses. To avoid excessive force on the suspension, the hydraulic piston can be equipped with pressure relief valves, as used in passive shock absorbers. During these simulations, a maximum torque due to hydraulic loads of 1.2 Nm and a maximum radial force of 60 N were recorded on the spool.

Electromagnetic design

The angular motion of the valve spool is achieved using a custom-designed permanent magnet synchronous motor. The diameter of the machine was set to fulfill the envelope of the sleeves. The machine cross section was optimized in COMSOL Multiphysics by means of parametric variations to yield the maximum torque-to-length ratio. Subsequently, its active length was adapted to achieve a continuous torque of 0.7 Nm and a maximum torque of 2.4 Nm for less than 10 s.[22] These values are deemed sufficient to overcome the contributions of inertial and friction on the spool during operation. To save space in the axial direction, a concentrated winding was adopted in a nine-slot, 10-pole configuration, which yields an elevated winding factor.[23] The machine winding was designed to achieve a base speed of 650 rpm at peak torque, with a DC link supply of 12 V (vehicle battery voltage). This speed is sufficient to reach a full spool stroke of 30° in only 7.7 ms, which proves to be sufficient to control suspension dynamics, with frequencies of interest below 30 Hz.

Figure 6 depicts the PMSM magnetic flux density distribution while yielding a continuous torque output. The layout of the winding is also shown. The machine operates unsaturated, below an average flux density of 1.4 T in the teeth and the back iron yoke. The relevant dimensions and machine parameters are listed in Table 1.

Table 1. Electric machine design features.

Feature	Value	Unit
Permanent magnet material	N45SH NdFeB	–
Magnetic circuit material	M270-35A steel	–
Number of stator slots	9	–
Number of magnet poles	10	–
Stator outside diameter	60	Mm
Rotor outside diameter	25.2	Mm
Air gap length	0.5	Mm
Active length	36	Mm
Max. magnet thickness	3	Mm
Tooth width	6.2	Mm
Slot depth	14.1	Mm
Slot opening	2	Mm
Winding layout	Wye, series	–
Number of turns per coil	16	–
Number of strands in hand	6	–
Wire gage	0.5	Mm
Peak torque	2.4	Mm
Peak phase current amplitude	33.4	A
DC-link voltage	12	V
Peak power	163	W
Base speed	650	rpm
Permanent magnet flux linkage	9.93	mWb
Inductance (*d* and *q* axes)	0.33	mH
Phase resistance	82.6	mΩ

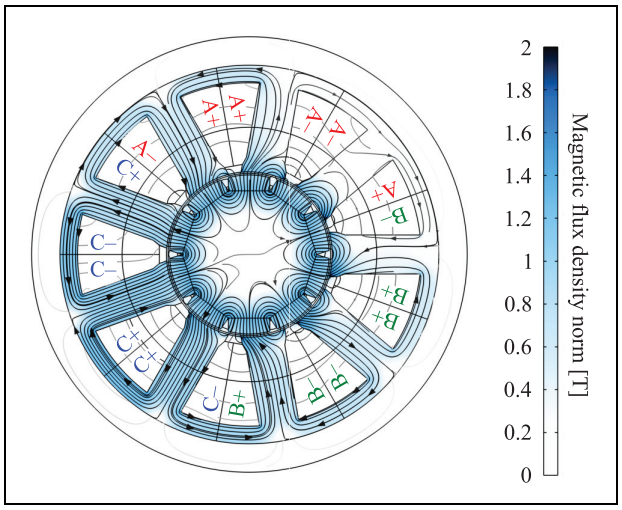

Figure 6. Magnetic flux density distribution (color map) and magnetic vector potential isocurves for the designed electric machine during continuous operation. Letters in the slots indicate the winding pattern for phases A, B, C.

The proposed electric machine ensures an ideally linear torque production using field-oriented current control:

$$T = \frac{3}{2} p \lambda_{\mathrm{p}} i_{\mathrm{q}} \tag{4}$$

where λ_{p} is the permanent-magnet flux linkage, p the number of rotor pole pairs and i_{q} the quadrature-axis current. Spools involving linear motion require reluctance-based actuators, which introduce important drawbacks. The solenoid force output is unidirectional and requires a return spring to provide opposite but asymmetric force action.[24,25] This unidirectional force is usually approximated as

$$F_{\mathrm{s}} \cong K_{\mathrm{s}} \frac{i_{\mathrm{s}}^2}{g^2} \tag{5}$$

being K_{s} a proportionality constant depending on the magnetic circuit properties, i_{s} the solenoid current, and g the air gap between the mover and the stator. Note that the device is benefited in terms of output force for large input currents and small air gaps. However, since the air gap changes with the stroke, the behavior of the output force is stroke-dependent and highly nonlinear. Additionally, in a vehicle application, a linear-displacement spool is sensitive to external perturbations due to the natural oscillation induced by road irregularities.

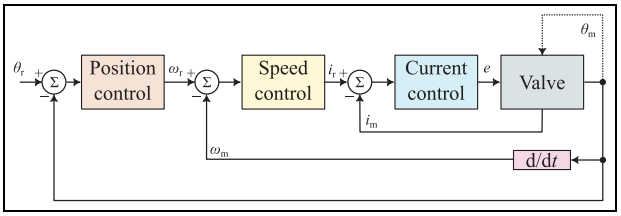

Figure 7. Nested loop approach for the motion control of the rotary valve prototype.

Rotary valve control

To guarantee precise spool angle tracking, a cascade loop architecture is adopted, where current, speed and position control loops are sequentially nested (see Figure 7). The inner current loop is closed through field-oriented control, which allows tracking current reference in direct (d) and quadrature (q) axes with respect to the magnet poles. The angular position of the rotor is needed to operate in d, q axes. Since the operational speed always remains below the base speed, no field weakening is applied to the electric machine. Thereby, the current reference in the d axis is always null, whereas the q-axis setpoint is imposed to reach a target torque. The current reference in the q axis comes from a mid speed loop, which employs the time derivative of the spool position to track a speed set-point. This value is determined by a third, outer position loop. Spool position references come from a lookup table that maps the actuator working point (output force at a specific suspension speed) with the necessary valve aperture. Force targets may be calculated using any damper control strategy, such as skyhook

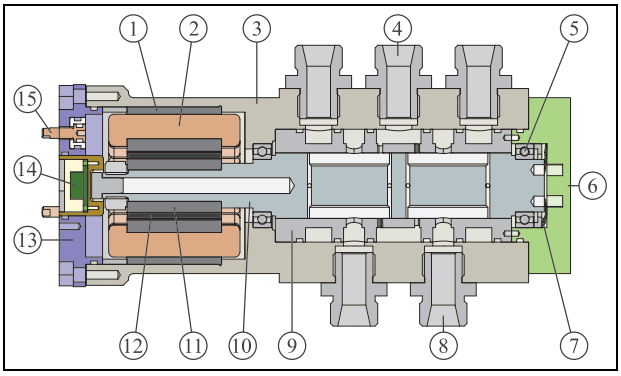

Figure 8. Rotary valve assembly cross section: (1) stator stack, (2) winding coil (×9), (3) casing, (4) rail port (×3), (5) ball bearing (×2), (6) valve cover, (7) wave spring, (8) damper port (×2), (9) sleeve, (10) spool, (11) rotor stack, (12) permanent magnet (×10), (13) motor cover, (14) position sensor, (15) phase plug (×3).

control.[26] For this application, current, speed and position compensators are proportional-integral (PI).

Assembly

The assembly cross section in Figure 8 shows the integration of the rotary valve. This system combines the valve and electric machine subsystems inside a pressure-tight aluminum casing (3). The electric machine is composed of a stator with laminated stack (1) and windings (2), and a rotor with iron stack (11) and permanent magnets (12). The motor requires a position sensor (14) for control purposes. The hydraulic circuit presents a rotary spool made of steel (10) supported by two ball bearings (5) in x arrangement and preloaded by a wave spring (7). The shaft of the spool is extended to support the rotor of the electric machine. To avoid friction losses, no gaskets or seals are added in between these two systems. Then, all elements inside the casing share the same pressurized oil medium. This choice allows for a compact and highly integrated valve design. Custom phase plugs (15) are provided with o-rings to avoid fluid leakages toward the exterior. The motor cover (13) is made of anodized aluminum to prevent short circuits between phases. The steel sleeve (9) is fixed to a cover on the valve side (6) through two pins. Standardized threaded ports are used to connect pressure rails (4) to an external motor-pump unit, and hydraulic chamber ports (8) to the actuator.

Quarter-car simulations

Before proceeding with the physical production of a prototype, the proposed system is validated numerically on the quarter car model of an E-class luxury sedan. This model is equipped with a numerical representation of the actuator. Skyhook and groundhook techniques are applied to test comfort and road holding performance, respectively, while traveling through an ISO-C class road at 70 km/h. Active control cases are compared against the same vehicle equipped with a passive suspension. This numerical implementation is represented in Figure 9.

For simplicity, the two rails p_0 and p_1 are considered ideal pressure sources. The valve is modeled as variable orifices. Discharge coefficients are fitted from CFD simulations to reproduce accurately the behavior of the valve. In addition, reaction hydraulic forces and torques are extracted from CFD results and applied to the valve as a function of the spool angular position. Two pressure-relief valves are used to limit the actuator output force to 3 kN.

The rotary valve is position-controlled. Its angular set-point is calculated through feedback and feed-forward approaches. The former one uses damper pressure values to estimate the actuator force. This value is compared against a force reference F_r and fed through a proportional controller. Feed-forward, on the other

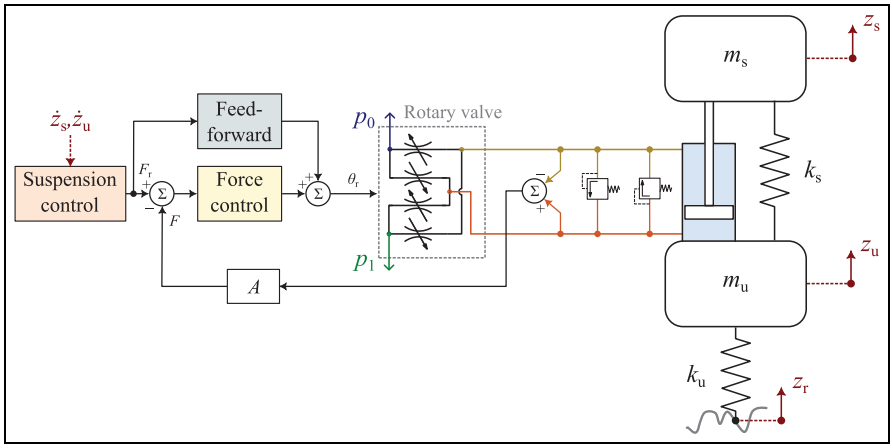

Figure 9. Numerical model of a quarter car with rotary valve-based active suspension. The suspension is represented as a force-controlled hydraulic actuator. The force control receives a set-point F_r from a suspension control law and it determines a valve opening command θ_r.

Table 2. E-class luxury sedan quarter car parameters.

Feature	Symbol	Value	Unit
Sprung mass	m_s	446.3	Kg
Unsprung mass	m_u	46.5	kg
Passive damping	c_p	7.24	Ns/mm
Spring stiffness	k_s	29.22	N/mm
Tire stiffness	k_u	278	N/mm

Table 3. Performance results for an E-class sedan with active and passive suspensions.

Suspension	Damping $\left[\left(\frac{Ns}{mm}\right)\right]$			rms($\ddot{z}_w$)	rms(η_{rh})
	c_p	c_1	c_2	[(m/s^2])]	[(−])]
Passive	7.24	0	0	2.01	0.24
Skyhook	0	10.8	0.8	0.80	0.39
Groundhook	0	3	4	1.49	0.21

hand, considers a precalculation of the output force as a function of the angular position of the spool and the suspension speed. This look-up table can be obtained from CFD models.

To evaluate performance indices related to comfort and road-holding, the active valve model is introduced in a quarter car model using the parameters listed in Table 2. The passive damping value can be replaced by an active control law. A generalized suspension force control method obeys the following law:

$$F_r = -c_1\dot{z}_s + c_2\dot{z}_u \tag{6}$$

The selection of damping coefficients c_1 and c_2 may suit specific control objectives, such as comfort or road holding. The former is indicated by the root-mean-square (RMS) value of a weighted acceleration $\ddot{z}_w$ obtained by filtering the sprung mass acceleration $\ddot{z}_s$ with a band-pass function that resembles the sensitivity of the human body to vertical vibrations.[27] The latter is evaluated by the RMS value of the road holding index η_{rh}, defined as the ratio between the tire force and the weight of the vehicle. For both indices, better performances correspond to lower values. Table 3 summarizes the tested configurations and the obtained results for each case. The skyhook control law is seen to prioritize comfort, thereby yielding a significantly lower RMS acceleration on the vehicle chassis at the cost of increasing the road holding index. In contrast, the groundhook strategy tends to favor road holding. In these regards, the active suspension outperforms the passive one.

Experiments

Test rig setup

Following the described mechanical assembly, a valve prototype was built. To characterize the valve, a hydraulic circuit was also designed with the objective of reproducing the pressure supply and piping depicted in Figure 1. The resulting test rig is shown in Figure 10.

Rail pressures p_1 and p_0 are established using a fixed displacement pump (Marzocchi 1PD115, 8 cm^3/rev, 4), driven by an industrial motor drive (Kollmorgen AKM5x motor, 7, and AKD inverter). The shafts of both machines are coupled by means of an elastic joint (R + W EK1).

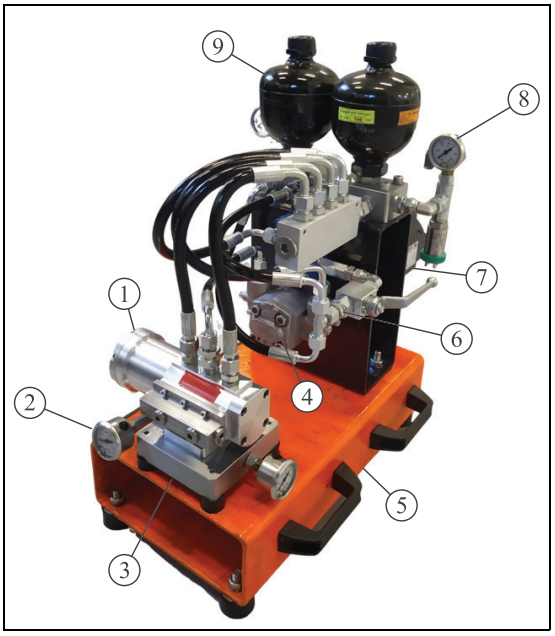

Figure 10. Test bench layout: (1) valve, (2) actuator pressure gage (×2), (3) hydraulic manifold, (4) hydraulic pump, (5) frame, (6) pressure-relief valve, (7) electric motor, (8) rail pressure gage (×2), and (9) hydraulic accumulator (×2).

The valve in test (1) is mounted on a steel manifold (3) with two hydraulic channels that represent the actuator ports (p_r, p_c). The pressures in these channels are measured using two analog gages (2).

A solid frame (5) is used to support the entire test bed. The motor-pump unit is supported through a metallic flange. The frame is also used to support a steel manifold designed to distribute the two pressure lines generated by the hydraulic pump to the rail ports. Furthermore, a pressure-relief valve (Bosch-Rexroth, 6) is connected in parallel to the motor-pump group for safety purposes. Two additional pressure gages (8) are connected to the pump rails for measurement purposes. Finally, two gas accumulators (9) are mounted on each

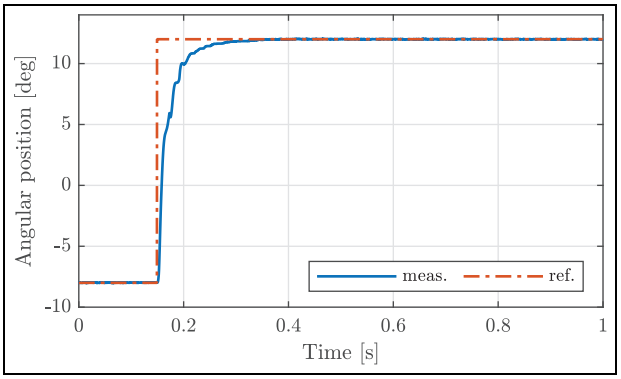

Figure 11. Experiment: valve position step response.

rail to attenuate pressure fluctuations. The filling and preload of the oil in the circuit are performed manually through a hand pump placed outside the bench and connected to the main manifold when required.

Valve control validation

The valve electric machine is controlled using Texas Instruments hardware (LAUNCHXL F28379D control board and BOOSTXL DRV8323RS inverter). The control firmware is produced using automatic code generation in Simulink, for rapid prototyping. PI loops are tuned by starting from the current compensator, which is the fastest and most critical control in the machine. In this case, the current controllers for the d and q axes are set to attain a bandwidth of 1 kHz, following a zero-pole cancelation approach in the winding impedance terms. Subsequently, the speed and position loops were calibrated heuristically and validated through two tests. In these preliminary experiments, the valve prototype is preloaded with oil, but the actuator ports are totally closed.

Figure 11 illustrates the experimental response of the valve when an angular step reference of 12° is imposed, starting from an initial condition of −8°. The obtained behavior is over-damped because no overshoot occurs. Furthermore, the rise time, defined at 90% of the total stroke (20°), is reached under 52 ms.

A more realistic position profile was produced by simulating an E-class vehicle traveling on an ISO C-class road[28] at 70 km/h, while a comfort-oriented skyhook control is applied to one of the corners of the vehicle. This working condition represents a worst-case scenario for the actuator in terms of angular command effort. Figure 12 shows the results of this test in the time and frequency domains. Reference and measured time histories of the spool angular position demonstrate that the valve performs strokes close to its full range of 30°. Tracking performance is favorable, with an RMS error of 2.2° throughout the profile. In addition, the frequency spectrum of the spool position shows intense activity around 1.16 Hz and 11.8 Hz, which can be directly related to the natural frequencies of the sprung and unsprung masses, respectively. In this instance, slight attenuation is observed around the unsprung mass natural frequency due to limitations in the position controller bandwidth.

Results in Figures 11 and 12 highlight the advantages of using a rotary valve, where precise position tracking is available through motion control. When using a solenoid spool, a displacement sensor should be installed to guarantee proportional control with the obtained degree of accuracy. The use of a return spring is useful to avoid the position transducer, at the cost of lowering dramatically the bandwidth, thus penalizing the dynamic response of the actuator in a relatively fast application.

Static characterization

After tuning the position control of the valve, the setup is tested with the actuator ports blocked. The purpose of this test is to verify the ability of the actuator to exert active forces at null suspension speed that is, standstill

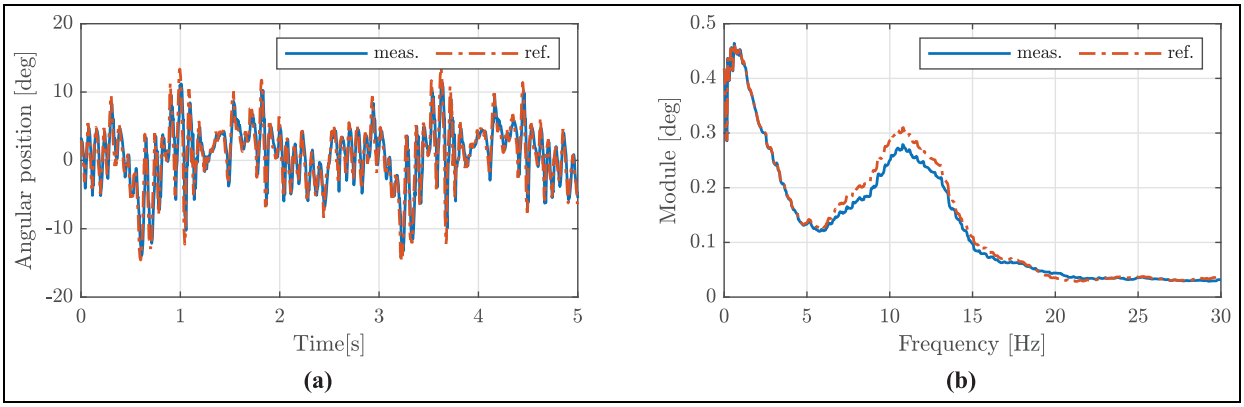

Figure 12. Experiment: valve position response to an irregular reference profile representing the spool activity when an E-class vehicle travels on an ISO C-class road at 70 km/h, while a comfort-oriented skyhook control is applied on the suspension corner. (a) Time history and (b) frequency response.

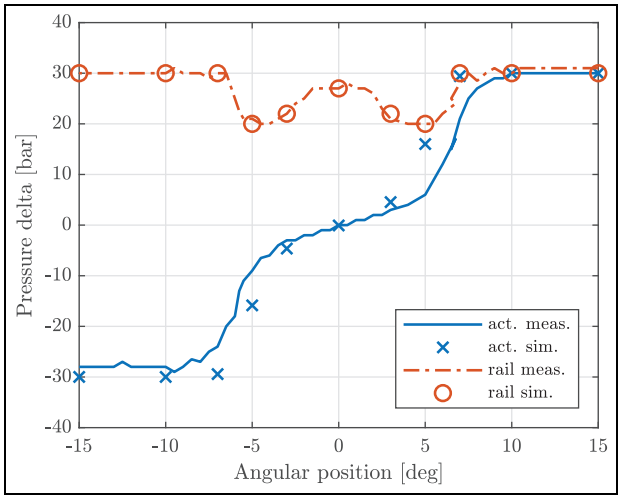

Figure 13. Experiment: Static characterization results of the prototype. Pressure delta on the rail and actuator as a function of the spool angular position. The variations of the actuator pressure delta underline the ability of the device to exert active forces at standstill.

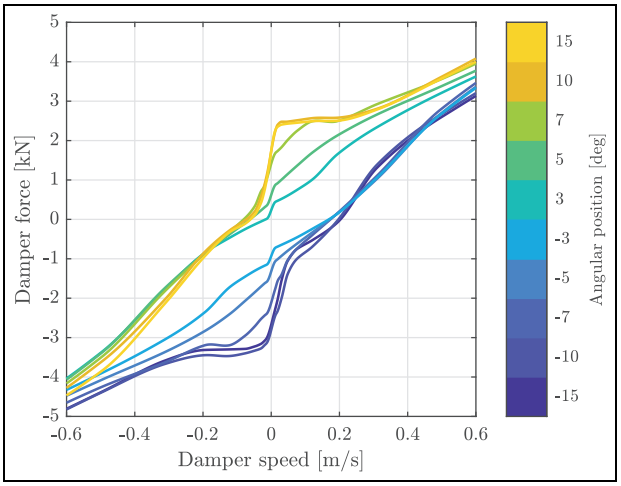

Figure 14. Experiment: Force-speed characteristic of the actuator under dynamic testing. A sinusoidal actuator stroke is imposed at variable frequency, while the spool angular position is fixed according to the color scale.

condition. These forces are related to the delta pressure across the hydraulic actuator: $p_r - p_c$.

For this experiment, the hydraulic circuit is manually preloaded at 20 bar and the servomotor pump unit is driven at fixed angular speeds up to 2000 rpm to keep a minimum pressure delta between the rails of 20 bar ($p_1 - p_0$). Furthermore, the valve is position controlled assuming fixed and stepped angular values in the $\pm 15°$ range.

The resulting characteristic is shown in Figure 13, in which the experimental pressure drops are compared with the simulations. Due to the inability of the rail to hold a constant pressure drop, CFD simulations were carried out by matching the rail pressures with those measured experimentally. Specifically, central positions are critical because the valve imposes a hydraulic short circuit on the pump. This low-impedance condition produces elevated angular speeds on the driving pump, thus exceeding the operating limits of the device.

With adjustment of CFD responses that match the experimental rail pressures, a favorable match of the static pressure delta is observed. Since the obtained behavior is highly nonlinear, discrepancies are found where the derivative of the response is large. These mismatches can be attributed to machining tolerances of the spool and sleeve, as well as a slight misalignment of the internal valve components.

Dynamic characterization

The static conditions-characterized set-up was hydraulically connected to a linear actuator and installed on a damper test bench, thus reproducing the full actuator configuration. The test bench is set to impose a sinusoidal displacement profile with a stroke amplitude of 50 mm, while the frequency is changed to produce speed amplitudes ranging from 12 mm/s to 600 mm/s. Meanwhile, the valve is controlled to provide fixed angular positions. Following an initial preload of 20 bar, different valve apertures are tested, as seen in Figure 14. Again, in this case, the rail pressure experiences fluctuations, especially in center stroke position of the valve. For this reason, the damper force levels reached do not match those obtained from the CFD simulations in Figure 5. However, behavioral trends are confirmed in the four quadrants with respect to the valve angular position.

Taking into account an experimental average rail pressure drop of 30 bar and a numerical counterpart of 40 bar, an increase in force of 33% is expected in the experimental results. For example, at null damper speed, a maximum active force of 4.25 kN is expected.

To validate the responsiveness of the position control, a second dynamic test was performed by fixing the actuator at the null suspension stroke and applying a spool angular position frequency sweep with sine amplitudes of . and 10°.

The results obtained in this test appear in Figure 15. Position control guarantees zero error at 3 Hz when the reference signal has an amplitude of 5°. Slight attenuation is advised when the amplitude of the reference signal is duplicated. However, the module of the function is always above −3 dB throughout the tested frequency range. These results confirm the suitability of the valve to track angular references in the bandwidth of interest for a vehicle suspension. The force output results in Figure 15 confirm that lower apertures lead to lower force output. In this case, attenuation is stronger than in the position tracking case, but this could also be related to the limitations observed for the imposed rail pressures.

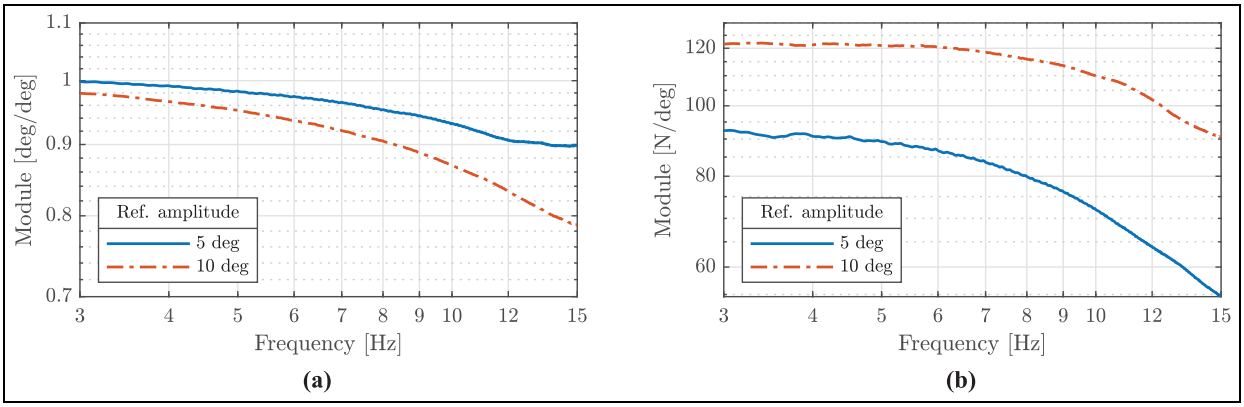

Figure 15. Experiment: Frequency response function of (a) the valve spool position and (b) the actuator output force when applying a sinusoidal spool position reference sweep from 3 to 15 Hz at . and 10° of amplitude. The hydraulic actuator position is locked.

Conclusions

This work proposed a novel fully active suspension system based on a rotary valve capable of establishing a controllable pressure drop between fixed pressure rails and a hydraulic cylinder. The behavior of the valve was illustrated and tested numerically at component and vehicle level. The selection of a rotary configuration was motivated in terms of the size of the solution, the electromagnetic features of the device and the required accuracy and responsiveness.

A prototype was designed to fit a compact envelope, where the valve is actuated by means of a highly integrated permanent-magnet synchronous motor. A prototype was built and tested, showing favorable performance in terms of actuation bandwidth. The force output of the proposed system was tested under static and dynamic conditions. Limitations were found due to the difficulty in fixing rail pressures to design values. However, within the tested pressure ranges, the device was able to fulfill its expected force output. Future developments of this work will include testing the proposed actuation system on a vehicle demonstrator.

Acknowledgments

The authors thank Piero Conti, Fabio Cotto, and Luca Bistolfi at Way Assauto for their valuable support throughout this research activity.

Declaration of conflicting interests

The author(s) declared no potential conflicts of interest with respect to the research, authorship, and/or publication of this article.

Funding

The author(s) disclosed receipt of the following financial support for the research, authorship, and/or publication of this article: Pablo Tapia is funded by Tecnologico de Monterrey (grant A01769991), and Consejo Nacional de Humanidades, Ciencias y Tecnologias (scholarship 1050445). This work was funded by Way Assauto in the context of a private research contract between the company and both universities (Tecnologico de Monterrey and Politecnico di Torino).

ORCID iD

Renato Galluzzi https://orcid.org/0000-0001-6125-8222

References

1. Savaresi SM, Poussot-Vassal C, Spelta C, et al. *Semi-active suspension control design for vehicles*. Oxford, UK: Elsevier, 2010.
2. Tseng HE and Hrovat D. State of the art survey: active and semi-active suspension control. *Veh Syst Dyn* 2015; 53(7): 1034–1062.
3. Yu M, Evangelou SA and Dini D. Advances in active suspension systems for road vehicles. *Engineering* 2024; 33: 160–177.
4. Nguyen DN and Nguyen TA. The dynamic model and control algorithm for the active suspension system. *Math Probl Eng* 2023; 2023(1): 9.
5. Mohd Riduan AF, Tamaldin N, Sudrajat A, et al. Review on active suspension system. *SHS Web Conf* 2018; 49: 02008.
6. Lee J, Oh K and Yi K. A novel approach to design and control of an active suspension using linear pump control–based hydraulic system. *Proc IMechE, Part D: J Automobile Engineering* 2020; 234(5): 1224–1248.
7. Asadi E, Ribeiro R, Khamesee MB, et al. Analysis, prototyping, and experimental characterization of an adaptive hybrid electromagnetic damper for automotive suspension systems. *IEEE Trans Vehicular Technol* 2017; 66(5): 3703–3713.
8. Gysen BLJ, van der Sande TPJ, Paulides JJH, et al. Efficiency of a regenerative direct-drive electromagnetic active suspension. *IEEE Trans Vehicular Technol* 2011; 60(4): 1384–1393.
9. Li Z, Zuo L, Luhrs G, et al. Electromagnetic energy-harvesting shock absorbers: design, modeling, and road

tests. *IEEE Trans Vehicular Technol* 2013; 62(3): 1065–1074.
10. Galluzzi R, Circosta S, Amati N, et al. Rotary regenerative shock absorbers for automotive suspensions. *Mechatronics* 2021; 77: 102580.
11. Dai J, Chang L, Qin Y, et al. Design and analysis of electromagnetic linear actuation-energy-reclaiming device applied to a NEW-TYPE energy-reclaiming suspension. *Actuators* 2023; 12(4): 142.
12. Nguyen TA. Advance the stability of the vehicle by using the pneumatic suspension system integrated with the hydraulic actuator. *Lat Am J Solids Struct* 2021; 18: e403.
13. Cytrynski S, Neerpasch U, Bellmann R, et al. The active suspension of the newMercedes-Benz GLE. *ATZ Worldw* 2018; 120(12): 42–45.
14. Reybrouck K, Vandersmissen B and Six K. ACOCAR: Ultimate comfort and safety through the energy-efficient active damping system of Tenneco. In: *21st Aachen colloquium automobile and engine technology*, Aachen, Germany: Aachener Kolloquium, 2012. pp.1–15.
15. Babawuro AY, Tahir NM, Muhammed M, et al. Optimized state feedback control of quarter car active suspension system based on LMI algorithm. *J Phys Conf Ser* 2020; 1502(1): 012019.
16. Kim J. *Hydrodynamic focusing micropump module with PDMS/nickel-particle composite diaphragms for microfluidic systems*. Master's Thesis, Louisiana State University and Agricultural and Mechanical College, 2011.
17. Lu Y, Huang Y, Zhen R, et al. Modelling and experimental validation of an adaptive interconnected suspension with adjustable roll stiffness (AIS-ARS). *Veh Syst Dyn* 2024; 0(0): 1–19. DOI: 10.1080/00423114.2024.2387782.
18. Rosam N and Darling J. Development and simulation of a novel roll control system for the interconnected hydragas® suspension. *Veh Syst Dyn* 1997; 27(1): 1–18.
19. Comber DB, Slightam JE, Gervasi VR, et al. Design, additive manufacture, and control of a pneumatic MR-Compatible needle driver. *IEEE Trans Robot* 2016; 32(1): 138–149.
20. Fite KB, Mitchell JE, Barth EJ, et al. Design and characterization of a rotary actuated hot gas servovalve. In: *Fluid power systems and technology*. Anaheim, CA: ASME, 2004, pp.63–69.
21. Öhlins. DFV Technology. https://www.ohlins.com/en-us/technologies/dfv-technology (2020, accessed 15 December 2024).
22. Dorrell DG, Hsieh MF, Popescu M, et al. A review of the design issues and techniques for radial-flux brushless surface and internal rare-earth permanent-magnet motors. *IEEE Trans Ind Electron* 2011; 58(9): 3741–3757.
23. Carraro E, Bianchi N, Zhang S, et al. Design and performance comparison of fractional slot concentrated winding spoke type synchronous motors with different slot-pole combinations. *IEEE Trans Ind Appl* 2018; 54(3): 2276–2284.
24. Manca R, Ruzimov S, Galluzzi R, et al. Enhancement of electromechanical load-leveling suspensions for automotive applications using reversible transmission mechanisms. *Mechatronics* 2024; 102: 103229.
25. Castellanos Molina LM, Galluzzi R, Hegde S, et al. Active electromagnetic clutch for crankshaft decoupling from a belt drive system. *Appl Sci* 2024; 14(11): 4770.
26. Genta G and Morello L. *The automotive chassis: volume 2: system design*. Cham, Switzerland: Springer Nature, 2019.
27. Zhang ZPL. Energy harvesting, ride comfort, and road handling of Regenerative Vehicle Suspensions. *ASME J Vib Acoust* 2013; 135(1): 011002.
28. ISO 8608:1995. Mechanical vibration – road surface profiles – reporting of measured data. 2011.